nature photonics

REVIEW ARTICLE

PUBLISHED ONLINE: 28 SEPTEMBER 2014 | DOI: 10.1038/NPHOTON.2014.220

Instabilities, breathers and rogue waves in optics

John M. Dudley[1], Frédéric Dias[2], Miro Erkintalo[3] and Goëry Genty[4]*

Optical rogue waves are rare, extreme fluctuations in the value of an optical field. The term 'optical rogue wave' was first used in the context of an analogy between pulse propagation in an optical fibre and wave group propagation on deep water, but has since been generalized to describe many other processes in optics. This Review provides an overview of the field, concentrating primarily on propagation in optical fibre systems that exhibit nonlinear breather and soliton dynamics, but also discussing other optical systems in which extreme events have been reported. Although statistical features such as long-tailed probability distributions are often considered to be the defining feature of rogue waves, we emphasize the underlying physical processes that drive the appearance of extreme optical structures.

Many physical systems exhibit behaviour associated with the emergence of high-amplitude events that occur with low probability but that have dramatic impact. Perhaps the most widely known examples of such processes are the giant oceanic 'rogue waves' that emerge unexpectedly from the sea with great destructive power[1]. There is general agreement that the physics behind the generation of giant waves is different from that of usual ocean waves, although there is a general consensus that one unique causative mechanism is unlikely. Indeed, oceanic rogue waves have been shown to arise in many different ways: from linear effects such as directional focusing or the random superposition of independent wave trains, to nonlinear effects associated with the growth of surface noise to form localized wave structures[1,2].

The analogous physics of nonlinear wave propagation in optics and hydrodynamics has been known for decades, and the focusing nonlinear Schrödinger equation (NLSE) applies to both systems in certain limits (Box 1). However, the description of instabilities in optics as rogue waves was first used in 2007 when Solli *et al.* reported long-tailed histograms in measurements of intensity fluctuations at long wavelengths in fibre supercontinuum (SC) spectra[3]. An analogy between this optical instability and oceanic rogue waves was suggested for two reasons. First, highly skewed distributions are often considered to define extreme processes, as they predict that high-amplitude events far from the median are still observed with non-negligible probability[4]. Second, the particular regime of SC generation being studied developed from modulation instability (MI), a nonlinear process associated with the exponential amplification of noise that had previously been proposed as a mechanism for generating ocean rogue waves[2].

These pioneering results not only enabled a quantitative analysis of fluctuations at the spectral edge of a broadband SC, but also motivated many subsequent studies into how large-amplitude structures could emerge in optical systems. These studies attracted broad interest and essentially opened up a new field of 'optical rogue wave physics'. Although most research since has focused on wave propagation in optical fibres — particularly in regimes analogous to hydrodynamics — the term 'optical rogue wave' has now been generalized to describe other noisy processes in optics with long-tailed probability distributions, regardless of whether they are observed in systems with a possible oceanic analogy. Moreover, particular analytic solutions of the NLSE that describe solitons on a finite background — often called 'breathers' — are now also widely referred to as rogue wave solutions, even when studied outside a statistical context for mathematical interest, or when generated experimentally from controlled initial conditions. These wider definitions have become well-established, but can unfortunately lead to difficulty for the non-specialist.

Our aim here is to remove any possible confusion by presenting a synthetic review of the field, not in terms of its chronological development, which has been discussed elsewhere[5,6], but rather by classifying rogue waves in terms of their generating physical mechanisms. We begin by discussing rogue waves in the regime of NLSE fibre propagation where MI and breather evolution dominate the dynamics, and then discuss how the effects of perturbations to the NLSE can lead to the emergence of background-free solitons. This provides a natural lead-in to a discussion of the physics and measurement techniques of rogue solitons in fibre SC generation. Finally, we describe the techniques used to control the dynamics of rogue waves in fibre systems, followed by a survey of the results achieved in other systems: lasers and amplifiers, in which dissipative effects are central to the dynamics, and spatial systems, in which both nonlinear and linear dynamics can play a role.

Rogue waves and statistics

Before considering specific examples of optical rogue waves, we first briefly review how rogue wave events are manifested in the statistics of the particular system under study.

In optics, statistical properties are defining features of light sources. For example, the random intensity fluctuations of polarized thermal light follow an exponential probability distribution, and the intensity fluctuations of a laser above threshold follow a Gaussian probability distribution[7]. It was the experimental observation of 'L-shaped' long-tailed distributions[3] that first linked nonlinear optics with the wider theory of extreme events. In a sense, the presence of long-tailed distributions in optics should not be a surprise, as it is well-known that a nonlinear transfer function will modify the probability distribution of an input signal. Indeed, an exponential probability distribution in intensity is transformed under exponential gain to a power-law Pareto distribution. There are other cases, however, in which the functional nonlinear transformation of an input field cannot be identified, because the emergence of high-amplitude events arises from more complex dynamics. Optical rogue waves and long-tailed statistics have been observed in systems that exhibit both types of behaviour.

Rogue waves in optics have been identified in a number of different ways. One approach uses the idea from probability

[1]Institut FEMTO-ST, UMR 6174 CNRS-Université de Franche-Comté, Besançon, France, [2]School of Mathematical Sciences, University College Dublin, Belfield, Dublin 4, Ireland, [3]Department of Physics, The University of Auckland, Auckland 1142, New Zealand, [4]Department of Physics, Tampere University of Technology, Tampere, Finland. *e-mail: goery.genty@tut.fi

Box 1 | The optical–ocean analogy.

The analogy between the dynamics of ocean waves and pulse propagation in optical fibres arises from the central role of the NLSE in both systems. Figure B1 gives the governing equations and illustrates characteristic soliton solutions for both cases. In optics, the NLSE describes the evolution of a light pulse envelope modulating an electric field, whereas for deep water it describes the evolution of a group envelope modulating surface waves. It is important not to oversimplify or exaggerate this analogy. For example, the deep-water NLSE in oceanography does not describe the shape of individual wave cycles but only their modulating envelope. Thus, specific envelope solutions of the deep water NLSE cannot be considered physically as individual rogue waves; within the narrowband approximation of the NLSE, there will always be multiple surface waves underneath this envelope.

Recent studies into optical rogue waves in the MI and breather regime have motivated similar water-wave experiments[112,113], even to the extent of testing the resistance of scale models of maritime vessels to particular NLSE breather solutions[114]. Interestingly, higher-order effects described by an extended NLSE can also be present in deep water[115–117], and wave-tank experiments have even shown a form of hydrodynamic SC and soliton fission[118]. Note, however, that although a clear analogy between ocean wave and optical propagation exists in the unperturbed NLSE regime, there is no such rigorous analogy for the extended NLSE because the physical forms of the higher-order perturbations are very different.

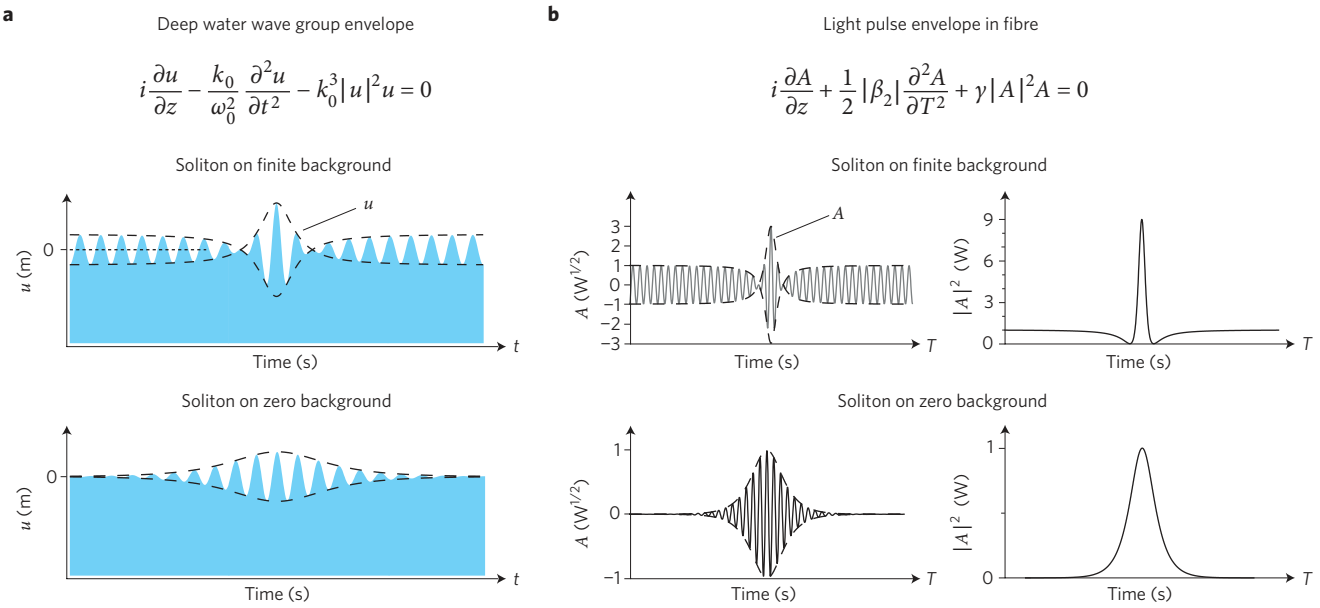

Figure B1 | The NLSE describes wave evolution in different physical systems. a, Wave group envelope u on deep water. **b**, Light pulse envelope A in an optical fibre with anomalous group velocity dispersion. The figure illustrates solitons on finite background (top) and solitons on zero background (bottom). Note that for the ocean wave case, there is always deep water underneath $u(z, t)$. For the water wave NLSE, k_0 is the wavenumber and ω_0 is the carrier frequency; for the fibre NLSE, $\beta_2 < 0$ is the group velocity dispersion and γ is the nonlinear coefficient. The usual NLSE for water waves in fact has time and space interchanged, but in this case the coefficients must be adapted[2].

theory that associates rogue events with particular extreme-value probability distributions, and such functions have provided good fits to the tails of optical intensity fluctuation histograms[8–10]. Another approach adapts the oceanographic definition of a rogue wave, whose trough-to-crest height H_{RW} satisfies $H_{RW} \gtrsim 2H_{1/3}$, where $H_{1/3}$ is the significant wave height, the mean height of the highest third of waves[11]. In optics, however, the accessible data is not the field amplitude but rather the intensity, and such data can take a variety of forms: an intensity time series; the levels of a two-dimensional camera image; or the space–time intensity evolution of an optical field. From this data, the intensity peaks are analysed statistically to compute a histogram, and the oceanographic definition is modified to define a threshold $I_{RW} \gtrsim 2I_{1/3}$, where the 'significant intensity' $I_{1/3}$ is the mean intensity of the highest third of events. This definition, although somewhat arbitrary, has been applied in several studies[12–15].

From a general perspective, the most interesting question is whether events in the distribution tail for a particular system arise from the same physics as those of events closer to the distribution median. This is also relevant in a practical context, as the ability to identify the conditions that cause extreme events is crucial to their prediction and control.

Modulation instability and breather dynamics

Modulation instability is a fundamental property of many nonlinear dispersive systems that is associated with the growth of periodic perturbations on a continuous-wave (CW) background[16]. In the initial evolution of MI, the spectral sidebands associated with the instability experience exponential amplification at the expense of the pump, but the subsequent dynamics are more complex and display cyclic energy exchange between multiple spectral modes. In optics, MI seeded from noise results in a series of high-contrast peaks of random intensity[17,18], and it is these localized peaks that have been compared with similar structures seen in studies of ocean rogue waves[2,19,20]. Significantly, the growth and decay dynamics of MI in the NLSE have exact solutions in the form of various types of breathers or 'solitons on finite background' (SFB)[21], allowing analytic studies into the conditions that favour the emergence of rogue waves.

SFBs constitute a class of NLSE solutions whose real and imaginary parts are linearly related. SFB solutions include Akhmediev breathers (ABs), Kuznetsov-Ma (KM) solitons, the Peregrine soliton (PS), and even more generally the bi-periodic solutions of the NLSE described by Jacobi elliptic functions[21–23]. Many of these solutions have been labelled as 'rogue waves'[24], although this interpretation must be made with great care; as we will see below, the statistical criterion for rogue waves in an MI field seeded by noise is generally only satisfied by particular higher-order SFB solutions (sometimes referred to as multi-rogue waves or higher-order rogue waves)[25–28].

Before discussing noise-seeded MI in detail, we first describe these SFBs and breather solutions by referring to the dimensionless NLSE:

$$i\frac{\partial\psi}{\partial\xi}+\frac{1}{2}\frac{\partial^2\psi}{\partial\tau^2}+|\psi|^2\psi=0 \qquad (1)$$

The envelope $\psi(\xi,\tau)$ is a function of propagation distance (ξ) and co-moving time (τ). Equation (1) can be related to the dimensional fibre-optic NLSE in Fig. B1 by defining a timescale $T_0=(|\beta_2|L_{NL})^{1/2}$ and a nonlinear length $L_{NL}=(\gamma P_0)^{-1}$, where β_2 is the group velocity dispersion, γ is the nonlinear coefficient and P_0 is the optical background power. The dimensional field $A(z,T)$ is $A=(P_0)^{1/2}\psi$, where dimensional time is $T=\tau T_0$ and dimensional distance is $z=\xi L_{NL}$. Analytic solutions of MI dynamics have been obtained by several authors[20–23,29–31], with the relevance to optics first pointed out by Akhmediev and Korneev[30]. The particular solution that describes MI growth and decay is[21,30]:

$$\psi(\xi,\tau)=e^{i\xi}\left[1+\frac{2(1-2a)\cosh(b\xi)+ib\sinh(b\xi)}{\sqrt{2a}\cos(\omega\tau)-\cosh(b\xi)}\right] \qquad (2)$$

The properties of this solution are determined by the positive parameter a ($a\neq0.5$) through arguments $b=[8a(1-2a)]^{1/2}$ and $\omega=2(1-2a)^{1/2}$. This solution is the AB when $0<a<0.5$; we observe evolution from the trivial plane wave ($a=0$) to a train of localized pulses with temporal period $\Delta\tau=\pi/(1-2a)^{1/2}$ (ref. 30). The AB solution provides an analytic framework for MI, where the real parameter ω corresponds to the modulation frequency and the real parameter b gives the parametric gain coefficient[32].

Figure 1a plots solutions for different values of a, and it is the spatial and temporal localization properties of these solutions that have led to their association with rogue waves. The MI instability growth rate is maximal at $a=0.25$, but increasing a actually leads to stronger localization in both dimensions until the limit $a\to0.5$, which gives the PS[23].

The PS, given by $\psi(\xi,\tau)=e^{i\xi}[1-4(1+2i\xi)/(1+4\tau^2+4\xi^2)]$, corresponds to a single pulse with localization in time (τ) as well as along the propagation direction (ξ) as shown, and it has maximal

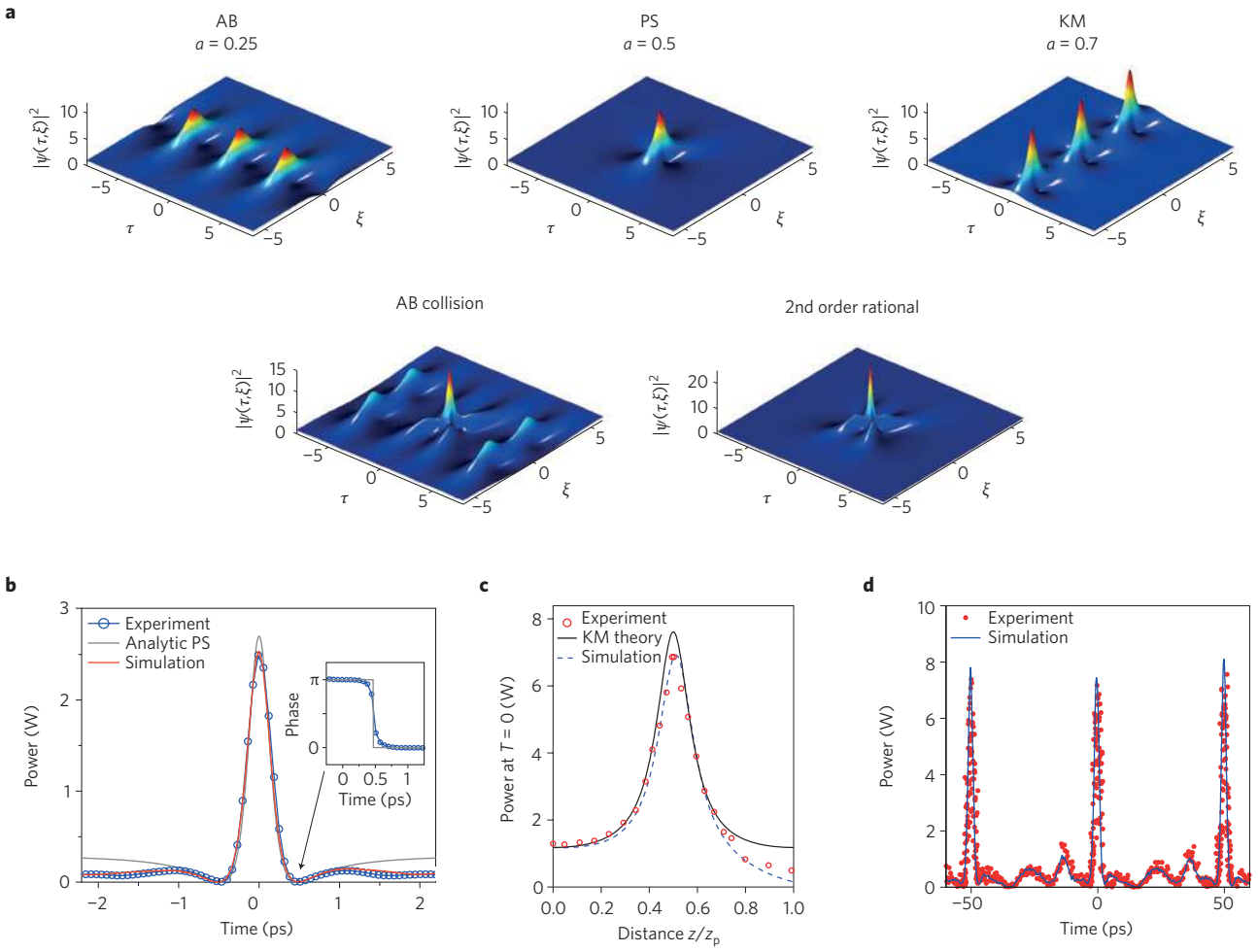

Figure 1 | SFB solutions of the NLSE. a, Analytical SFB solutions of equation (2) for varying parameter a. AB collision and the second-order rational soliton (or second-order PS) are also shown. **b**-**d**, Experimental results. **b**, Temporal PS properties asymptotically approached for $a=0.42$ (ref. 39). **c**, KM dynamics along the propagation direction for $a=1$ (ref. 42). Experiments, simulations and theory are compared in **b** and **c**. Here $z_p=5.3$ km, which corresponds to one period of the KM cycle. **d**, Comparison of experiments and simulations of a second-order solution for the collision of two ABs ($a=0.14$ and $a'=0.34$)[35]. AB, Akhmediev breathers; KM, Kuznetsov-Ma; PS, Peregrine soliton.

intensity among the AB solutions with $|\psi_{PS}|^2 = 9$. When $a > 0.5$, the parameters ω and b become imaginary, and the solution exhibits localization in the temporal dimension τ but periodicity along the propagation direction ξ. This is the KM soliton[22,29], which is shown in Fig. 1a for $a = 0.7$. In this regard, we note that the KM result of ref. 22 was the first reported mathematical SFB solution to the NLSE.

Each of the solutions described by equation (2) is a special case of a more general family of solutions that exhibit periodicity in both transverse time τ and longitudinal propagation direction ξ (ref. 21). More complex higher-order solutions also exist with even stronger localization and higher intensities than the PS[21], such as higher-order rational solitons[25–28,33] and AB collisions[34]. Figure 1a shows examples of both types of solutions[25,35,36].

The analytical results above have been used to design experiments with controlled initial conditions to excite particular SFB dynamics in fibre optics. The use of optical fibres provides an especially convenient experimental platform because the dispersion and nonlinearity parameters can be conveniently matched to available optical sources, thus yielding a propagation regime in which the NLSE is a valid model for the dynamics. Experiments typically involve the injection of a multi-frequency field into a nonlinear fibre — similar to the method developed for coherent pulse-train generation in telecommunications[37,38]. Figure 1b–d shows a selection of results obtained using this technique. The first experiments in 2010 used frequency-resolved optical gating to show localization in the PS regime[39], with measured intensity and phase agreeing well with numerical and analytical predictions (Fig. 1b). Later experiments examined in more detail the growth and decay of spectral amplitudes during AB evolution[40]. As pointed out by Van Simaeys *et al.*, the reversible dynamics of MI is a clear manifestation of Fermi–Pasta–Ulam recurrence in optics[41].

Experiments that excite KM-like evolution along the propagation direction have also been realized; Fig. 1c illustrates the growth and decay of the peak temporal intensity[42]. In another experiment, spectral shaping of an optical frequency comb synthesized initial conditions to excite the collision of two ABs[35]. Figure 1d shows an example of the results obtained, comparing the measured collision profile at the fibre output with numerical simulation. These results are significant because they highlight how collisions can yield significantly larger intensities than the elementary ABs alone, even exceeding the PS limit. Note that excited AB collision dynamics can be considered to be a particular case of higher-order MI, wherein the simultaneous excitation of multiple instability modes within the MI gain bandwidth gives rise to the nonlinear superposition of ABs[21,43–45].

The use of a modulated input field in these experiments means that the initial conditions correspond to a truncated Taylor series expansion of the analytic AB or PS far from the point of maximum localization, or an approximation to the ideal KM profile at the point of minimal intensity in its evolution cycle. The use of non-ideal initial conditions induces differences compared with the ideal dynamics (for example, the occurrence of multiple Fermi–Pasta–Ulam recurrence cycles for an AB), but simulations have shown that the spatiotemporal localization and field properties at the point of highest intensity remain well-described by the corresponding analytic SFB solution[46].

The experiments above give insight into how appropriate initial conditions can excite a range of analytic SFB structures in an NLSE system. These results are important in the study of rogue waves because structures very similar to those described by equation (2) (and their higher-order extensions) also appear in chaotic fields when MI develops from noise[33,34,47,48]. We illustrate this in Fig. 2

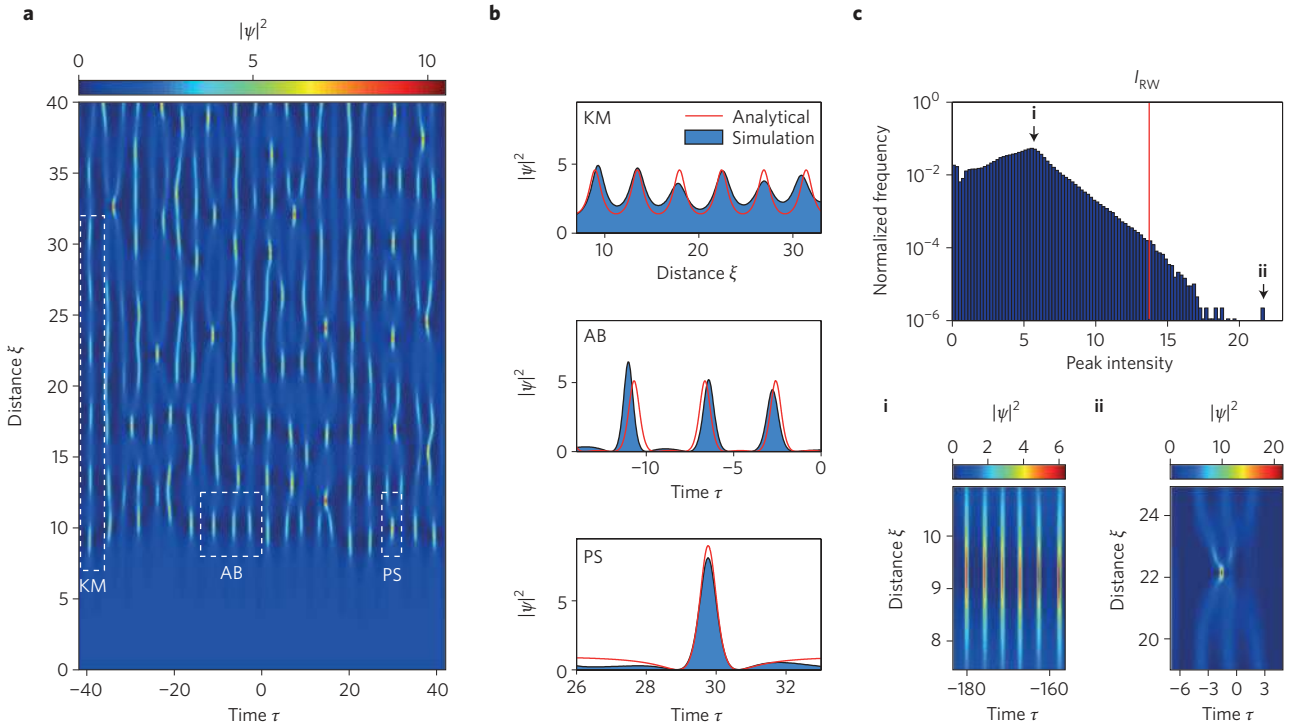

Figure 2 | Numerical simulation showing signatures of analytic NLSE solutions in chaotic MI. a, Density map showing the long-term temporal evolution of a chaotic field triggered by one-photon-per-mode noise superimposed on a continuous-wave background. Signatures of SFB solutions can be observed in the dynamics as indicated. **b**, Line profiles extracted from the regions of the chaotic field indicated by white dashed rectangles in **a**, compared with analytical NLSE solutions (red solid line). **c**, Peak-intensity statistics using an eight-connected neighbourhood regional maximum search to identify two-dimensional peaks from a wider simulation window. The maximum of the probability density corresponds to AB-like solutions at the peak of the MI gain, whereas the most extreme outliers arise from collisions of ABs. The bottom subfigures show the evolution of two events from different regions of the histogram (i) and (ii) as indicated. The initial amplitude of the field $\psi(\xi, \tau) = 1$.

using numerical simulations of the dimensionless NLSE, where clear signatures of the SFB solutions (periodicity in τ or along ξ, τ–ξ localization, the peak intensity value) can be identified when MI is triggered from a broadband noise background. Figure 2a plots a density map of the evolution as a function of distance ξ, showing emergence of an irregular series of temporal peaks around $\xi \sim 10$. Note that the average temporal periodicity here is $\Delta\tau \sim 2^{1/2}\pi$, which corresponds to the reciprocal of the frequency of maximum MI gain. After the initial emergence of these localized peaks, we see more complex periodic growth and decay behaviour along ξ.

Examining particular features of the evolution map reveals signatures of the analytic KM, AB and PS solutions described above, as plotted in Fig. 2b. For the KM region, a line profile of the evolution along ξ agrees well with the analytic result expected for a KM soliton; in the AB and PS regions, the temporal localization characteristics also agree well with corresponding analytic predictions. Of course, observing ideal analytic SFB structures is not expected given the random initial conditions, but it is remarkable how the analytic solutions can be mapped closely to the noise-generated structures. In this context, we remark that recent results have also considered different initial forms of small perturbations to the CW background and found similar signatures of AB structures[50].

These results confirm that SFB solutions can provide analytical insight into structures emerging from noise-seeded MI, but understanding their significance to the physics of rogue waves requires an analysis of the associated statistics[33,34]. To this end, Fig. 2c plots a histogram of the intensities of the localized peaks in a larger computational window (around 10^6 peaks in the τ–ξ plane). First, we note that the histogram maximum corresponds to an intensity of $|\psi|^2 = 5.6$, which is close to the AB intensity at maximal gain when $a = 0.25$. The fact that these structures appear more frequently than others in the chaotic regime is also consistent with experiments studying the spectral characteristics of spontaneous MI[18].

Second, we note an exponential tail (linear on a semi-logarithmic scale) for higher-intensities; the dashed line indicates the point in the tail that corresponds to the rogue wave intensity threshold $I_{RW} \sim 13$. It is interesting to remark here that the elementary AB and PS structures (with an intensity less than $I_{PS} = |\psi_{PS}|^2 = 9$) actually have intensities below the intensity I_{RW}, which suggests caution in the description of these solutions as rogue waves[24,39]. Approximately 2.5% of the total peaks have an intensity that exceeds the PS limit of $I_{PS} = 9$, and these events correspond to AB collisions arising physically from the continuous range of frequencies amplified by MI[33,34]. In our simulations, the largest among them (which make up only 0.1% of the total) have intensities exceeding the rogue wave threshold I_{RW} and would thus clearly be described as rogue wave events according to any criteria used[2,51]. Note that the figures below the histogram in Fig. 2c show simulation results for (i) a typical AB

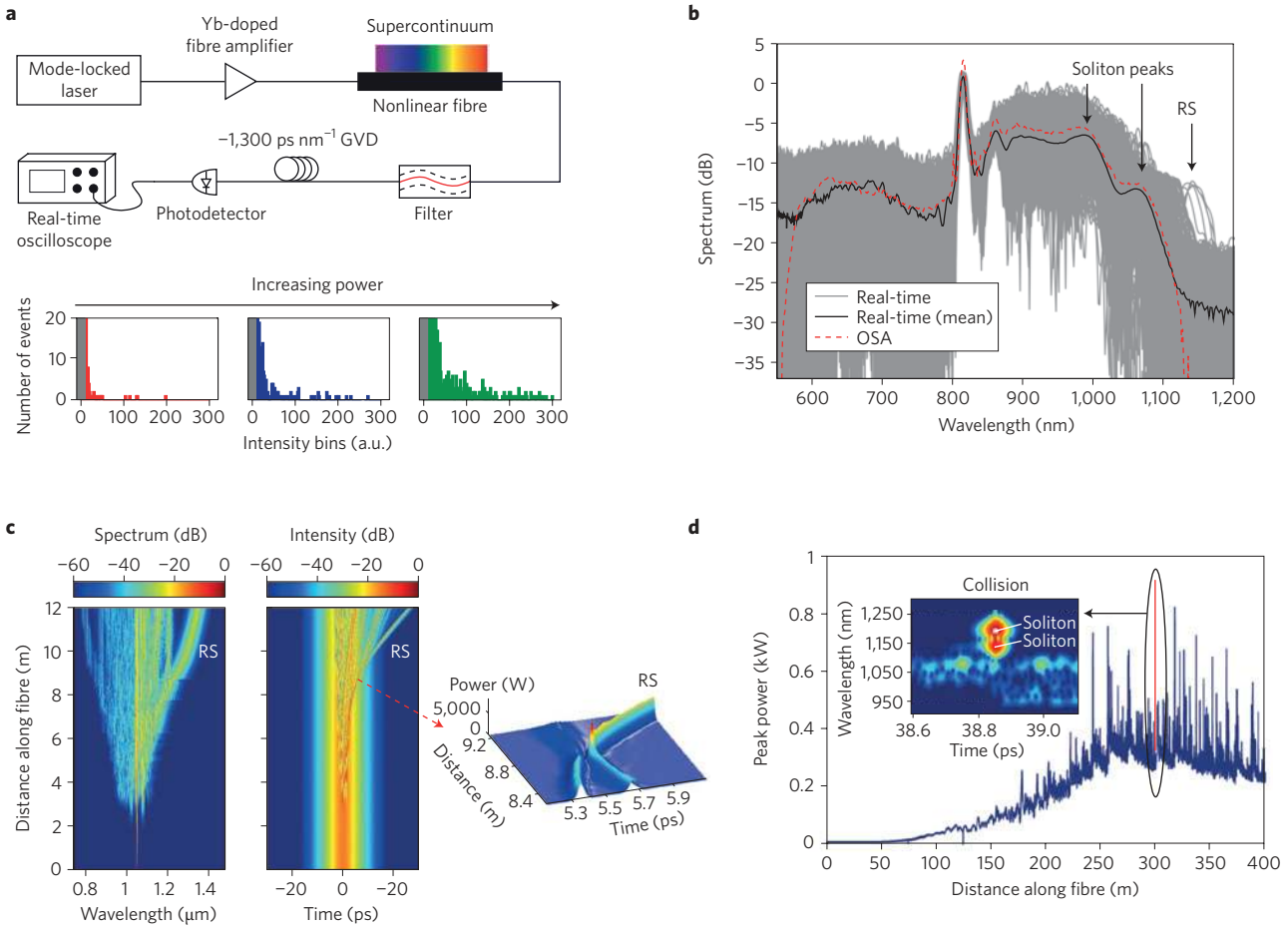

Figure 3 | Selection of experimental and numerical results for SC rogue solitons. a, Experimental set-up for the first optical rogue soliton (RS) measurements, together with long-wavelength intensity statistics at three different pump power levels[3]. GVD, group velocity dispersion. **b**, 1,000 single-shot SC spectra measured using dispersive Fourier transformation (grey), the computed mean (black) and the average spectrum measured with an optical spectrum analyser (OSA, red)[62]. **c**, Numerical simulations showing the spectral and temporal evolution of a rogue soliton in picosecond SC generation. Parameters from ref. 69. A rogue soliton emerges from the main spectrum at a propagation distance of 8.8 m. Two solitons collide at the same distance in the time-domain; energy transfer to one of the solitons yields the enhanced redshift. **d**, Evolution of peak intensity in numerical simulations of CW SC generation. The most intense events correspond to soliton collisions, with the time–frequency diagram (inset) illustrating a particular example[69].

solution and (ii) a three-breather collision from the distribution tail. Finally, we note that these results were obtained with a noise background of one photon per mode, although the exact fraction of highest-intensity events in the distribution tails may be expected to vary with the noise level used to seed MI[33,34].

Supercontinuum generation and solitons

The studies above show how SFB dynamics during fibre propagation can lead to strongly localized structures with rogue wave statistics. Interestingly, however, the first observations of rogue waves in optics were not made in the regime of SFB dynamics at all, but in 'long-pulse' SC generation. In this regime, higher-order effects beyond the basic NLSE played an important role[3], and although approximate SFB solutions can exist even under these conditions[52], the first observed rogue wave characteristics arose instead from the dynamics of background-free hyperbolic secant solitons.

Noise-seeded MI dynamics dominate the initial stages of long-pulse and CW SC generation, but the dynamics are significantly modified with propagation by higher-order dispersion and stimulated Raman scattering[32,49]. It is this perturbed dynamical evolution that drives the emergence of the rogue soliton characteristics of SC generation. Specifically, after initial evolution, which is statistically dominated by the AB with maximum gain (Fig. 2), perturbations cause the associated temporal peaks to reshape with further propagation into fundamental background-free hyperbolic secant solitons[18,53]. These sech-solitons then experience the additional dynamics of dispersive wave generation[54] and a continuous shift to longer wavelengths through the Raman effect[55]. Because the solitons emerge from a stochastic field of breather-like structures, their durations, amplitudes and wavelengths show considerable statistical variation. The strong dependence of the Raman self-frequency shift on duration[55], coupled with the effects of group velocity dispersion, therefore induces complex evolution involving multiple (stochastic) collisions and energy exchange between the solitons[56–59].

It has been known for many years[56] that such chaotic soliton dynamics could cause significant shot-to-shot noise in the SC spectrum, but it was the real-time measurement of these fluctuations[3] that first highlighted links to the field of extreme events. In this work, Solli *et al.* used a long-pass wavelength filter to select the portion of the SC spectrum in which they expected strong soliton intensity variations to occur, and then used dispersive Fourier transformation[60,61] to perform shot-to-shot measurements of the associated spectral fluctuations. The peaks in the resulting intensity time-series showed striking long-tailed statistics. Figure 3a shows the experimental set-up and a selection of recorded histograms at three different pump levels. The main conclusion drawn from these experiments was that the largest events in the tails of the histograms corresponded to a small number of 'rogue solitons' — solitons whose central wavelength had been Raman-shifted completely within the filter transmission band — which appeared as high-intensity events in the time series. More recently it has become possible to measure the full-bandwidth shot-to-shot SC spectra[62], and these experiments (Fig. 3b) have highlighted more directly the small number of extremely red-shifted rogue solitons.

Subsequent modelling and experiments examined in detail the dynamics that lead to such extreme frequency shifts, thereby clarifying the central role of soliton collisions[8,12,63–68]. Figure 3c shows numerical simulations that highlight the frequency- and time-domain properties of a particular rogue soliton event[69]. In the frequency domain, we see the transition from initial MI dynamics, with symmetric growth of noise-driven sidebands, to a regime in which distinct sech-soliton structures appear in the spectrum. A rogue soliton emerges at a distance of $z \sim 9$ m, and the snapshot of the time-domain evolution plot clearly illustrates a two-soliton collision at this point. The collision is associated with significant energy exchange (mediated by stimulated Raman scattering) to yield one higher-energy soliton (which then experiences a much greater Raman self-frequency shift) as well as a lower-amplitude residual pulse[12,63,69,70].

Note that although stimulated Raman scattering plays a central role for wave propagation in optical fibres, any perturbation that breaks NLSE integrability can cause a homogeneous initial state to self-organize into a large-scale, coherent rogue soliton as a result of multiple interactions with other solitons and dispersive waves[71]. Indeed, numerical studies have shown that higher-order dispersive perturbations alone can give rise to rogue solitons[59,68], provided that the incoherence in the system is not too large[48,72]. Although it may seem surprising, energy exchange between colliding solitons can occur even in this case, owing to resonant coupling between the solitons and radiation emitted during the collision[73].

Other numerical studies have investigated the statistical properties of SC rogue solitons in more detail. Several authors have considered the variation in local intensity along the propagation dimension, thereby showing that the intensity of colliding solitons at the point of collision can in fact be much higher than that of the rogue soliton at the fibre output[12,63,67]. Figure 3d shows this for the case of CW SC generation[67], where it is clear that the maximum intensity at certain points in the fibre is much higher than at the output. This suggests that significant differences may be observed between the statistical properties measured over the full field at all points of propagation and those measured at the fibre output. A detailed study of these differences has been reported, including a discussion of the effect of spectral filtering on the statistics[12]. We also note recent experimental work that uses dispersive Fourier transformation to examine the intensity correlation properties of both MI and SC, which has yielded further insights into the underlying dynamics[61,62,74]. Finally, we remark that although most studies in optics have focused on perturbation-induced collisions as a primary mechanism for generating extreme-frequency-shifting rogue solitons, the random emergence of coherent structures has been seen in numerical simulations of a basic NLSE model during the evolution of multimode CW fields with initial random phases[75].

Controlling rogue waves in fibre systems

The fact that SC rogue solitons have their origin in MI suggests the possibility to control their propagation using a dual-frequency input field such that the instability develops from a coherent modulation on the input envelope rather than from noise[32]. This approach is similar to that used to excite SFBs under controlled conditions.

The potential for seeding to stabilize the dynamics of rogue wave was first demonstrated experimentally by controlling picosecond SC generation with a frequency-shifted replica derived from the pump pulses[76]. The seed pulses, although only 0.01% as intense as the pump, caused a dramatic improvement in SC stability. Related numerical studies showed how an appropriate choice of seed frequency could significantly decrease the rogue soliton wavelength jitter while also increasing the overall SC bandwidth[77]. These results not only highlighted the potential of rogue soliton control for improving the performance of practical SC sources[8,77–79], but also stimulated ideas for enhancing spectral broadening in silicon waveguides[80]. Other experiments considered how seeding can improve the spectral properties of spontaneous MI, and remarkable spectral control has been demonstrated using CW seeding at only the 10^{-6} level[81]. One benefit of this technique is that it does not rely on the time-delay tuning required for picosecond seed pulses[82,83].

As well as controlling input conditions, other studies have shown that longitudinal variation in a fibre's dispersive and nonlinear properties can modify intensity fluctuations in both SC generation[84] and the dynamics of an evolving AB[85]. This work is significant because it shows how a modified fibre propagation environment can mimic the way in which ocean topography influences water wave propagation[1].

Amplifiers and lasers

In addition to the examples in conservative (or weakly dissipative) systems discussed above, rogue waves in systems with strong dissipation (gain or loss) have also been observed. Dissipative dynamics in optics have been studied for decades, and resonators, amplifiers and multimode lasers are well-known to exhibit a wide range of chaotic and self-organization effects[86]. However, the development of the field of optical rogue waves has now motivated the interpretation of these noise characteristics in terms of extreme-value processes.

Although dissipative systems do not generally have NLSE-governed hydrodynamic counterparts, exploring regimes of long-tailed statistics in such systems has nonetheless provided new insights into the underlying physical processes. The first observation of extreme events in a highly dissipative system reported long-tailed intensity statistics from Raman amplification of a coherent signal using an incoherent Raman pump[87]. The long-tailed statistics were attributed to the transfer of pump intensity fluctuations onto the coherent signal owing to the exponential dependence of Raman gain on pump intensity. Similar nonlinear noise transfer underlies the emergence of extreme-value statistics in fibre parametric amplifiers[88] and silicon waveguide Raman amplifiers[89,90]. Notably, Borlaug *et al.* explicitly calculated the power-law probability distribution function of the amplified signal intensity[89].

The complex noise characteristics of lasers in systems with external injection, mode-locking and delayed feedback is well-known, and it is not surprising that laser noise spiking behaviour can exhibit long-tailed statistics. Experiments have reported such properties in an erbium fibre laser with harmonic pump modulation[91], a CW Raman fibre laser[92], mode-locked Ti:sapphire and fibre lasers[14,93,94], and passively *Q*-switched lasers[95]. In Fig. 4 we illustrate an experimental result in which a sequence of highly localized temporal noise bursts was recorded from an erbium-doped mode-locked fibre laser; the associated intensity statistics show significant deviation from exponentially bounded distributions[14]. These experiments confirmed previous numerical studies that predicted intensity spikes in passively mode-locked fibre lasers through chaotic pulse bunching[13,96]. Rogue wave behaviour has also been seen from an optically injected semiconductor laser, where it was shown that the rogue wave dynamics could be described deterministically, with noise influencing only the probability of their observation[97] (similar to noise-seeded MI.)

These results are inspiring significant theoretical efforts to identify the mechanisms that induce extreme temporal localization[13,96] and to characterize instabilities in real-time[14,94,98]. However, it should be noted that many of the reported features of extreme laser fluctuations had probably been seen in earlier experiments without being recognized as a separate class of rogue wave instability[99,100].

Spatial instabilities

There has also been extensive interest in interpreting spatial instabilities in terms of extreme events. The first such study considered intensity noise in the output spatial mode of a cavity with nonlinear gain from an optically pumped liquid-crystal light valve[101]. Depending on the system parameters, the cavity exhibited complex transverse mode dynamics that, in the high-finesse limit, exhibited highly unstable oscillation behaviour with long-tailed statistics. The optical rogue-wave-like events were attributed to the nonlinear feedback and symmetry-breaking in the cavity design.

Optical filamentation — a complex process that involves self-focusing, plasma formation and temporal shaping dynamics — is another example of a spatially extended system that exhibits rogue wave statistics. Studies into filamentation have found different statistical behaviour depending on the particular parameter regime investigated. In the single-filament regime, shot-to-shot spectral fluctuations arising from pump noise transfer through self-phase modulation have demonstrated long-tailed statistics[9,102]. In the multifilament regime, where the transverse profile of the input beam is broken into multiple strands through spatial MI, localized structures obeying non-Gaussian statistics have been predicted[103]. Experiments and simulations studying filamentation in gas have revealed that local refractive index variations driven by nonlinearity can cause individual filament strings to merge, thereby giving rise to short-lived spatial rogue waves at the gas cell output[104]. Figure 5a shows the experimental set-up of this work, with numerical and experimental results shown in Fig. 5b,c.

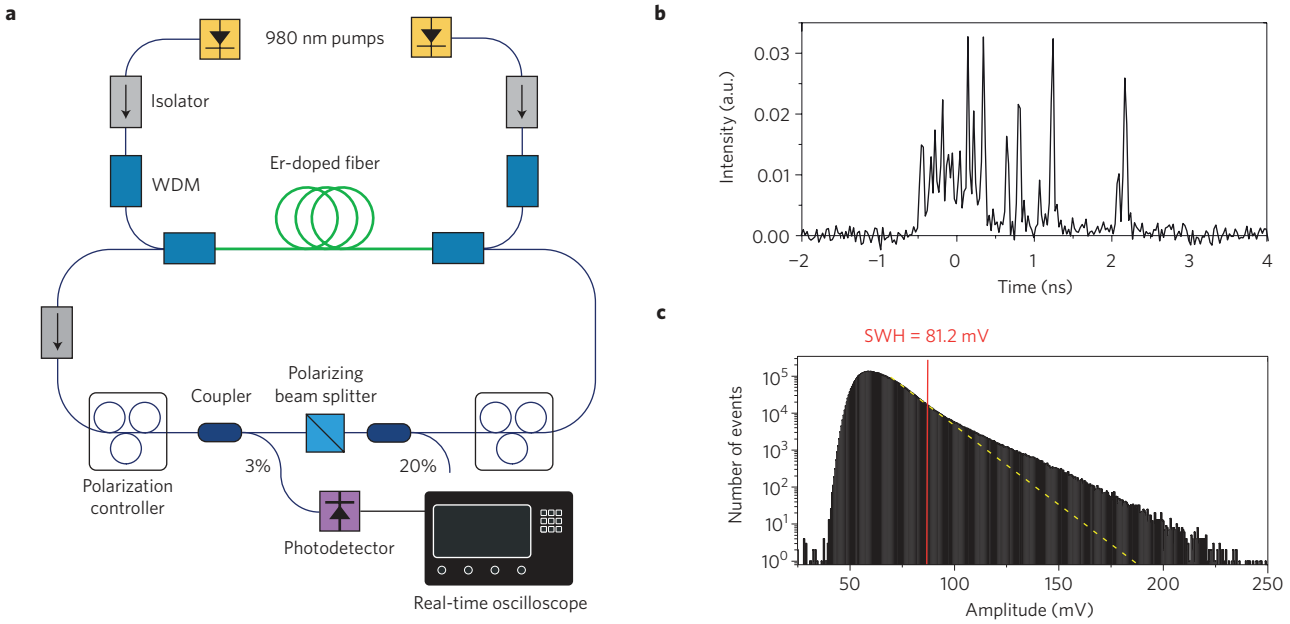

Figure 4 | Dissipative rogue waves. a, Schematic of an erbium-doped mode-locked fibre laser generating a train of temporally localized bursts of noise. WDM, wavelength-division multiplexer. **b**, Time-domain experimental measurement showing a chaotic pulse cluster emitted by the laser over a single round-trip. **c**, Peak intensity statistics over nearly 10 million round-trips. The red line shows the significant peak intensity, and the dashed yellow line corresponds to an exponentially bounded distribution. Figure reproduced with permission from ref. 14, © 2012 APS.

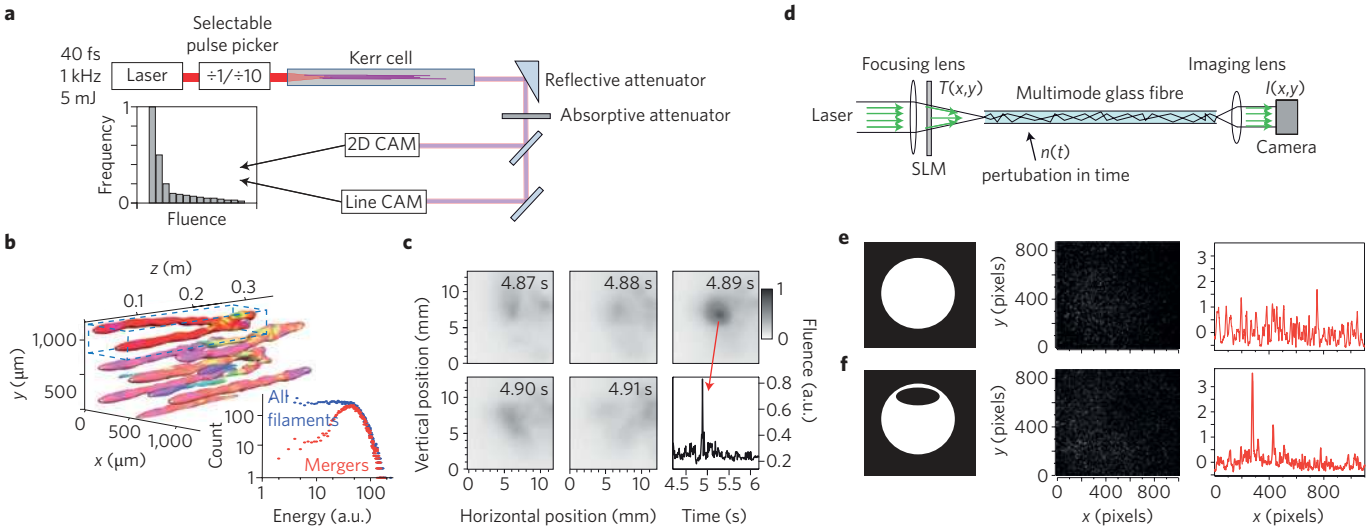

Figure 5 | Rogue waves in the transverse spatial plane of optical beams. a, Experimental set-up used to study multiple filamentation in a gas cell, with an example of observed fluence statistics. CAM, camera. **b**, Results of numerical simulations, which show how highly localized rogue structures can arise from the merging of individual filaments. **c**, Two-dimensional multifilament fluence profiles measured with a high-speed camera reveal a spatiotemporal rogue wave that appears 4.89 s after the start of the recording. **d**, Experimental set-up used to investigate rogue waves in the speckle pattern at the output of a multimode fibre. A spatial light modulator (SLM) is used to control the input beam profile. **e**,**f**, Measured speckle patterns (centre) and corresponding intensity distributions taken at a selected y-coordinate (right) when the SLM transmission mask (left) is uniform (**e**) and inhomogeneous (**f**). An optical rogue wave is observed in **f**. Figure reproduced with permission from: **a**–**c**, ref. 104, © 2013 APS; **d**–**f**, ref. 106, © 2011 APS.

Interestingly, long-tailed statistics have also been seen in linear spatial systems. In one experiment studying emission from a gigahertz microwave emitter array, researchers were able to probe the emitted electromagnetic field as a function of time and spatial position across the array[105]. Although the system contained no obvious nonlinear element, long-tailed distributions in the microwave intensity were observed. Another example of a linear system that exhibits rogue wave statistics in the transverse spatial plane (but here at visible frequencies) was found to be the speckle pattern observed at the output of a strongly multimode fibre[106]. In this system the asymmetry and inhomogeneity in the injected beam profile (Fig. 5d–f) yielded a sub-exponential intensity distribution that drove the emergence of rare high-intensity spots in the speckle pattern.

Discussion and outlook

The initial results of Solli *et al.* in 2007 firmly embedded the science of extreme events in the domain of optics, and we have seen how very different optical systems can exhibit strong localization and long-tailed statistics. However, a major conclusion of this Review is that the mechanisms driving the emergence of rogue wave behaviour in optics can be very different depending on the particular system studied, and we hope that the categorization provided here will assist in structuring future work in this field. We also remark that great care must be taken when comparing results obtained in different contexts. The particular example of optical fibre propagation is a case in point: the physics driving the excitation of analytical rogue wave breather solutions in a regime of propagation governed by the basic NLSE is significantly different from the perturbed-NLSE dynamics of extreme red-shifting rogue solitons in SC generation, and it is important to stress this distinction.

Although there is clearly intrinsic interest in studying extreme instabilities in optics, much of the motivation for studying rogue waves in optical systems has been to gain insight into the origin of their oceanic counterparts. In this regard, however, it is also essential to recognize that not all experiments in optics yield direct insight into ocean wave propagation. There are certain regimes of wave propagation on the ocean and in optical fibre that are well-described by a basic NLSE model; provided experiments are performed in these regimes before the onset of any perturbations, insights obtained in the different environments can be shared. In other cases, however, although the observation of long-tailed statistics in optics may be linked to the wider theory of extreme events in physics, it is simply incorrect to compare such instabilities with oceanic wave-shaping processes. Analogies can be powerful tools in physics, but they must be used with care[107].

That said, in regimes where the optical–ocean analogy is valid, there is of course intense interest in using optical experiments to improve our general understanding of rogue waves, and experiments in optics have indeed motivated similar studies in water wave tanks (Box 1). Although rogue waves on the ocean may arise in a number of different ways, these experiments provide convincing evidence that nonlinearities in the ocean can play a role in extreme wave emergence and must be included *a priori* in any consideration of potential high-amplitude ocean wave-shaping mechanisms. A particular advantage of optical systems is that the high repetition rate of optical sources allows the generation of large data sets such that even events occurring with extremely low probabilities can be studied[108].

Even in a strictly optical context, many open directions of research still remain. Experiments and modelling of optical rogue wave dynamics are providing new insights into how noise drives (and/or stabilizes) the dynamics of nonlinear optical systems, how energy exchange occurs during soliton interactions, and how novel measurement techniques can reveal noise correlations even in the very complex case of SC generation. It is interesting to remark in closing that there is also significant effort in optics to understand how effects like dispersion and nonlinearity engineering can allow optical systems to model different aspects of the ocean environment[109]. Indeed, recently developed 'topographic' fibres have already been shown to be capable of controlling both optical MI and soliton dynamics[110,111]. As research continues to progress in this field, it is likely that the noise properties across a number of optical systems may find analogies with areas of physics other than oceanography, thereby allowing the use of a convenient optical test bed with which to study a wide range of different physical processes.

Received 7 March 2014; accepted 22 August 2014; published online 28 September 2014

References

1. Kharif, C. & Pelinovsky, E. Physical mechanisms of the rogue wave phenomenon. *Eur. J. Mech. B* **22,** 603–634 (2003).
2. Osborne, A. R. *Nonlinear Ocean Waves and the Inverse Scattering Transform* (Academic Press, 2010).
3. Solli, D. R., Ropers, C., Koonath, P. & Jalali, B. Optical rogue waves. *Nature* **450,** 1054–1057 (2007).
4. Goldie, C. M. & Klüppelberg, C. in *A Practical Guide to Heavy Tails: Statistical Techniques and Applications* (eds Adler, R. L., Feldman, R. & Taqqu, M. S.) 435–459 (Birkhäuser, 1998).
5. Akhmediev, N., Dudley, J. M., Solli, D. R. & Turitsyn, S. K. Recent progress in investigating optical rogue waves. *J. Opt.* **15,** 060201 (2013).
6. Onorato, M., Residori, S., Bortolozzo, U., Montina, A. & Arecchi, F. T. Rogue waves and their generating mechanisms in different physical contexts. *Phys. Rep.* **528,** 47–89 (2013).
7. Goodman, J. W. *Statistical Optics* (John Wiley & Sons, 1985).
8. Dudley, J. M., Genty, G. & Eggleton, B. J. Harnessing and control of optical rogue waves in supercontinuum generation. *Opt. Express* **16,** 3644–3651 (2008).
9. Kasparian, J., Bejot, P., Wolf, J. P. & Dudley, J. M. Optical rogue wave statistics in laser filamentation. *Opt. Express* **17,** 12070–12075 (2009).
10. Demircan, A. *et al.* Rogue events in the group velocity horizon. *Sci. Rep.* **2,** 850 (2012).
11. Sverdrup, H. U. & Munk, W. H. Wind, sea and swell. Theory of relations for forecasting. *U. S. Navy Hydrographic Office Pub. 601* (1947).
12. Erkintalo, M., Genty, G. & Dudley, J. M. On the statistical interpretation of optical rogue waves. *Eur. Phys. J. Spec. Top.* **185,** 135–144 (2010).
13. Zaviyalov, A., Egorov, O., Iliew, R. & Lederer, F. Rogue waves in mode-locked fiber lasers. *Phys. Rev. A* **85,** 013828 (2012).
14. Lecaplain, C., Grelu, P., Soto-Crespo, J. M. & Akhmediev, N. Dissipative rogue waves generated by chaotic pulse bunching in a mode-locked laser. *Phys. Rev. Lett.* **108,** 233901 (2012).
15. Demircan, A. *et al.* Rogue wave formation by accelerated solitons at an optical event horizon. *Appl. Phys. B* **115,** 343–354 (2013).
16. Zakharov, V. E. & Ostrovsky, L. A. Modulation instability: The beginning. *Physica D* **238,** 540–548 (2009).
17. Kelleher, E. J. R., Travers, J. C., Popov, S. V. & Taylor, J. R. Role of pump coherence in the evolution of continuous-wave supercontinuum generation initiated by modulation instability. *J. Opt. Soc. Am. B* **29,** 502–512 (2012).
18. Dudley, J. M., Genty, G., Dias, F., Kibler, B. & Akhmediev, N. Modulation instability, Akhmediev breathers and continuous wave supercontinuum generation. *Opt. Express* **17,** 21497–21508 (2009).
19. Dyachenko, A. I. & Zakharov, V. E. Modulation instability of Stokes wave → freak wave. *JETP Lett.* **81,** 255–259 (2005).
20. Dysthe, K. B. & Trulsen, K. Note on breather type solutions of the NLS as models for freak-waves. *Phys. Scripta* **T82,** 48–52 (1999).
21. Akhmediev, N. & Ankiewicz, A. *Solitons: Non-linear Pulses and Beams* (Chapman & Hall, 1997).
22. Kuznetsov, E. Solitons in a parametrically unstable plasma. *Sov. Phys. Dokl.* **22,** 507–508 (1977).
23. Peregrine, D. H. Water-waves, nonlinear Schrödinger equations and their solutions. *J. Aust. Math. Soc. B* **25,** 16–43 (1983).
24. Shrira, V. I. & Geogjaev, V. V. What makes the Peregrine soliton so special as a prototype of freak waves? *J. Eng. Math.* **67,** 11–22 (2010).
25. Akhmediev, N., Ankiewicz, A. & Taki, M. Waves that appear from nowhere and disappear without a trace. *Phys. Lett. A* **373,** 675–678 (2009).
26. Dubard, P., Gaillard, P., Klein, C. & Matveev, V. B. On multi-rogue wave solutions of the NLS equation and positon solutions of the KdV equation. *Eur. Phys. J. Spec. Top.* **185,** 247–258 (2010).
27. Dubard, P. & Matveev, V. B. Multi-rogue waves solutions to the focusing NLS equation and the KP-I equation. *Nat. Hazards Earth Syst. Sci.* **11,** 667–672 (2011).
28. Kedziora, D. J., Ankiewicz, A. & Akhmediev, N. Classifying the hierarchy of nonlinear-Schrödinger-equation rogue-wave solutions. *Phys. Rev. E* **88,** 013207 (2013).
29. Ma, Y. C. Perturbed plane-wave solutions of the cubic Schrödinger equation. *Stud. Appl. Math.* **60,** 43–58 (1979).
30. Akhmediev, N. & Korneev, V. I. Modulation instability and periodic solutions of the nonlinear Schrödinger equation. *Theor. Math. Phys.* **69,** 1089–1093 (1986).
31. Henderson, K. L., Peregrine, D. H. & Dold, J. W. Unsteady water wave modulations: Fully nonlinear solutions and comparison with the nonlinear Schrödinger equation. *Wave Motion* **29,** 341–361 (1999).
32. Agrawal, G. P. *Nonlinear Fiber Optics* 5th edn (Academic Press, 2013).
33. Akhmediev, N., Ankiewicz, A. & Soto-Crespo, J. M. Rogue waves and rational solutions of the nonlinear Schrödinger equation. *Phys. Rev. E* **80,** 026601 (2009).
34. Akhmediev, N., Soto-Crespo, J. M. & Ankiewicz, A. Extreme waves that appear from nowhere: On the nature of rogue waves. *Phys. Lett. A* **373,** 2137–2145 (2009).
35. Frisquet, B., Kibler, B. & Millot, G. Collision of Akhmediev breathers in nonlinear fiber optics. *Phys. Rev. X* **3,** 041032 (2013).
36. Akhmediev, N., Eleonskii, V. M. & Kulagin, N. E. Generation of periodic trains of picosecond pulses in an optical fiber: exact solutions. *Sov. Phys. JETP* **62,** 894–899 (1985).
37. Tai, K., Tomita, A., Jewell, J. L. & Hasegawa, A. Generation of subpicosecond soliton-like optical pulses at 0.3 THz repetition rate by induced modulational instability. *Appl. Phys. Lett.* **49,** 236–238 (1986).
38. Greer, E. J., Patrick, D. M., Wigley, P. G. J. & Taylor, J. R. Generation of 2 THz repetition rate pulse trains through induced modulational instability. *Electron. Lett.* **25,** 1246–1248 (1989).
39. Kibler, B. *et al.* The Peregrine soliton in nonlinear fibre optics. *Nature Phys.* **6,** 790–795 (2010).
40. Hammani, K. *et al.* Spectral dynamics of modulation instability described using Akhmediev breather theory. *Opt. Lett.* **36,** 2140–2142 (2011).
41. Van Simaeys, G., Emplit, P. & Haelterman, M. Experimental demonstration of the Fermi–Pasta–Ulam recurrence in a modulationally unstable optical wave. *Phys. Rev. Lett.* **87,** 033902 (2001).
42. Kibler, B. *et al.* Observation of Kuznetsov–Ma soliton dynamics in optical fibre. *Sci. Rep.* **2,** 463 (2012).
43. Wabnitz, S. & Akhmediev, N. Efficient modulation frequency doubling by induced modulation instability. *Opt. Commun.* **283,** 1152–1154 (2010).
44. Erkintalo, M. *et al.* Higher-order modulation instability in nonlinear fiber optics. *Phys. Rev. Lett.* **107,** 253901 (2011).
45. Hammani, K. *et al.* Peregrine soliton generation and breakup in standard telecommunications fiber. *Opt. Lett.* **36,** 112–114 (2011).
46. Erkintalo, M., Genty, G., Wetzel, B. & Dudley, J. M. Akhmediev breather evolution in optical fiber for realistic initial conditions. *Phys. Lett. A* **375,** 2029–2034 (2011).
47. Coillet, A., Dudley, J. M., Genty, G., Larger, L. & Chembo, Y. K. Optical rogue waves in whispering-gallery-mode resonators. *Phys. Rev. A* **89,** 013835 (2014).
48. Kibler, B., Hammani, K., Michel, C., Finot, C. & Picozzi, A. Rogue waves, rational solitons and wave turbulence theory. *Phys. Lett. A* **375,** 3149–3155 (2011).
49. Dudley, J. M., Genty, G. & Coen, S. Supercontinuum generation in photonic crystal fiber. *Rev. Mod. Phys.* **78,** 1135–1184 (2006).
50. Zakharov, V. E. & Gelash, A. A. Nonlinear stage of modulation instability. *Phys. Rev. Lett.* **111,** 054101 (2013).
51. Akhmediev, N. & Pelinovsky, E. Introductory remarks on "Discussion & Debate: Rogue Waves – Towards a Unifying Concept?" *Eur. Phys. J. Spec. Top.* **185,** 1–4 (2010).
52. Ankiewicz, A., Soto-Crespo, J. M., Chowdhury, M. A. & Akhmediev, N. Rogue waves in optical fibers in presence of third-order dispersion, self-steepening, and self-frequency shift. *J. Opt. Soc. Am. B* **30,** 87–94 (2013).
53. Mahnke, C. & Mitschke, F. Possibility of an Akhmediev breather decaying into solitons. *Phys. Rev. A* **85,** 033808 (2012).
54. Wai, P. K. A., Menyuk, C. R., Lee, Y. C. & Chen, H. H. Nonlinear pulse-propagation in the neighborhood of the zero-dispersion wavelength of monomode optical fibers. *Opt. Lett.* **11,** 464–466 (1986).
55. Gordon, J. P. Theory of the soliton self-frequency shift. *Opt. Lett.* **11,** 662–664 (1986).
56. Islam, M. N. *et al.* Femtosecond distributed soliton spectrum in fibers. *J. Opt. Soc. Am. B* **6,** 1149–1158 (1989).
57. Frosz, M. H., Bang, O. & Bjarklev, A. Soliton collision and Raman gain regimes in continuous-wave pumped supercontinuum generation. *Opt. Express* **14,** 9391–9407 (2006).
58. Luan, F., Skryabin, D. V., Yulin, A. V. & Knight, J. C. Energy exchange between colliding solitons in photonic crystal fibers. *Opt. Express* **14,** 9844–9853 (2006).
59. Genty, G. *et al.* Collisions and turbulence in optical rogue wave formation. *Phys. Lett. A* **374,** 989–996 (2010).
60. Goda, K. & Jalali, B. Dispersive Fourier transformation for fast continuous single-shot measurements. *Nature Photon.* **7,** 102–112 (2013).
61. Solli, D. R., Herink, G., Jalali, B. & Ropers, C. Fluctuations and correlations in modulation instability. *Nature Photon.* **6,** 463–468 (2012).
62. Godin, T. *et al.* Real time noise and wavelength correlations in octave-spanning supercontinuum generation. *Opt. Express* **21,** 18452–18460 (2013).
63. Liu, C., Rees, E. J., Laurila, T., Jian, S. S. & Kaminski, C. F. An adaptive filter for studying the life cycle of optical rogue waves. *Opt. Express* **18,** 26113–26122 (2010).

64. Kibler, B., Finot, C. & Dudley, J. M. Soliton and rogue wave statistics in supercontinuum generation in photonic crystal fibre with two zero dispersion wavelengths. *Eur. Phys. J. Spec. Top.* **173,** 289–295 (2009).
65. Erkintalo, M., Genty, G. & Dudley, J. M. Rogue-wave-like characteristics in femtosecond supercontinuum generation. *Opt. Lett.* **34,** 2468–2470 (2009).
66. Lafargue, C. *et al.* Direct detection of optical rogue wave energy statistics in supercontinuum generation. *Electron. Lett.* **45,** 217–218 (2009).
67. Mussot, A. *et al.* Observation of extreme temporal events in CW-pumped supercontinuum. *Opt. Express* **17,** 17010–17015 (2009).
68. Taki, M. *et al.* Third-order dispersion for generating optical rogue solitons. *Phys. Lett. A* **374,** 691–695 (2010).
69. Antikainen, A., Erkintalo, M., Dudley, J. M. & Genty, G. On the phase-dependent manifestation of optical rogue waves. *Nonlinearity* **25,** R73–R83 (2012).
70. Driben, R. & Babushkin, I. Accelerated rogue waves generated by soliton fusion at the advanced stage of supercontinuum formation in photonic-crystal fibers. *Opt. Lett.* **37,** 5157–5159 (2012).
71. Dyachenko, A. I., Zakharov, V. E., Pushkarev, A. N., Shvets, V. F. & Yankov, V. V. Soliton turbulence in nonintegrable wave systems. *Zh. Eksp. Teor. Fiz. Sov. Phys. JETP* **96,** 2026–2032 (1989).
72. Hammani, K., Kibler, B., Finot, C. & Picozzi, A. Emergence of rogue waves from optical turbulence. *Phys. Lett. A* **374,** 3585–3589 (2010).
73. Buryak, A. V. & Akhmediev, N. N. Internal friction between solitons in near-integrable systems. *Phys. Rev. E* **50,** 3126–3133 (1994).
74. Wetzel, B. *et al.* Real-time full bandwidth measurement of spectral noise in supercontinuum generation. *Sci. Rep.* **2,** 882 (2012).
75. Turitsyn, S. K. & Derevyanko, S. A. Soliton-based discriminator of noncoherent optical pulses. *Phys. Rev. A* **78,** 063819 (2008).
76. Solli, D. R., Ropers, C. & Jalali, B. Active control of rogue waves for stimulated supercontinuum generation. *Phys. Rev. Lett.* **101,** 233902 (2008).
77. Genty, G., Dudley, J. M. & Eggleton, B. J. Modulation control and spectral shaping of optical fiber supercontinuum generation in the picosecond regime. *Appl. Phys. B* **94,** 187–194 (2009).
78. Solli, D. R., Jalali, B. & Ropers, C. Seeded supercontinuum generation with optical parametric down-conversion. *Phys. Rev. Lett.* **105,** 233902 (2010).
79. Solli, D. R., Ropers, C. & Jalali, B. Rare frustration of optical supercontinuum generation. *Appl. Phys. Lett.* **96,** 151108 (2010).
80. DeVore, P. T. S., Solli, D. R., Ropers, C., Koonath, P. & Jalali, B. Stimulated supercontinuum generation extends broadening limits in silicon. *Appl. Phys. Lett.* **100,** 101111 (2012).
81. Cheung, K. K. Y., Zhang, C., Zhou, Y., Wong, K. K. Y. & Tsia, K. K. Manipulating supercontinuum generation by minute continuous wave. *Opt. Lett.* **36,** 160–162 (2011).
82. Li, Q. *et al.* Investigating the influence of a weak continuous-wave-trigger on picosecond supercontinuum generation. *Opt. Express* **19,** 13757–13769 (2011).
83. Nguyen, D. M. *et al.* Incoherent resonant seeding of modulation instability in optical fiber. *Opt. Lett.* **38,** 5338–5341 (2013).
84. Kudlinski, A. *et al.* Control of pulse-to-pulse fluctuations in visible supercontinuum. *Opt. Express* **18,** 27445–27454 (2010).
85. Tian, Q., Yang, Q., Dai, C. Q. & Zhang, J. F. Controllable optical rogue waves: Recurrence, annihilation and sustainment. *Opt. Commun.* **284,** 2222–2225 (2011).
86. Haken, H. *Synergetics. Introduction and Advanced Topics* (Springer, 2004).
87. Hammani, K., Finot, C., Dudley, J. M. & Millot, G. Optical rogue-wave-like extreme value fluctuations in fiber Raman amplifiers. *Opt. Express* **16,** 16467–16474 (2008).
88. Hammani, K., Finot, C. & Millot, G. Emergence of extreme events in fiber-based parametric processes driven by a partially incoherent pump wave. *Opt. Lett.* **34,** 1138–1140 (2009).
89. Borlaug, D., Fathpour, S. & Jalali, B. Extreme value statistics in silicon photonics. *IEEE Photon. J.* **1,** 33–39 (2009).
90. DeVore, P. T. S., Solli, D. R., Borlaug, D., Ropers, C. & Jalali, B. Rogue events and noise shaping in nonlinear silicon photonics. *J. Opt.* **15,** 064001 (2013).
91. Pisarchik, A. N., Jaimes-Reategui, R., Sevilla-Escoboza, R., Huerta-Cuellar, G. & Taki, M. Rogue waves in a multistable system. *Phys. Rev. Lett.* **107,** 274101 (2011).
92. Randoux, S. & Suret, P. Experimental evidence of extreme value statistics in Raman fiber lasers. *Opt. Lett.* **37,** 500–502 (2012).
93. Kovalsky, M. G., Hnilo, A. A. & Tredicce, J. R. Extreme events in the Ti:sapphire laser. *Opt. Lett.* **36,** 4449–4451 (2011).
94. Runge, A. F. J., Aguergaray, C., Broderick, N. G. R. & Erkintalo, M. Raman rogue waves in a partially mode-locked fiber laser. *Opt. Lett.* **39,** 319–322 (2014).
95. Bonazzola, C., Hnilo, A., Kovalsky, M. & Tredicce, J. R. Optical rogue waves in an all-solid-state laser with a saturable absorber: Importance of the spatial effects. *J. Opt.* **15,** 064004 (2013).
96. Soto-Crespo, J. M., Grelu, P. & Akhmediev, N. Dissipative rogue waves: Extreme pulses generated by passively mode-locked lasers. *Phys. Rev. E* **84,** 016604 (2011).
97. Bonatto, C. *et al.* Deterministic optical rogue waves. *Phys. Rev. Lett.* **107,** 053901 (2011).
98. Runge, A. F. J., Aguergaray, C., Broderick, N. G. R. & Erkintalo, M. Coherence and shot-to-shot spectral fluctuations in noise-like ultrafast fiber lasers. *Opt. Lett.* **38,** 4327–4330 (2013).
99. Duguay, M. A., Hansen, J. W. & Shapiro, S. L. Study of Nd-glass laser radiation. *IEEE J. Quant. Electron.* **6,** 725–743 (1970).
100. Horowitz, M., Barad, Y. & Silberberg, Y. Noiselike pulses with a broadband spectrum generated from an erbium-doped fiber laser. *Opt. Lett.* **22,** 799–801 (1997).
101. Montina, A., Bortolozzo, U., Residori, S. & Arecchi, F. T. Non-Gaussian statistics and extreme waves in a nonlinear optical cavity. *Phys. Rev. Lett.* **103,** 173901 (2009).
102. Majus, D., Jukna, V., Valiulis, G., Faccio, D. & Dubietis, A. Spatiotemporal rogue events in femtosecond filamentation. *Phys. Rev. A* **83,** 025802 (2011).
103. Lushnikov, P. M. & Vladimirova, N. Non-Gaussian statistics of multiple filamentation. *Opt. Lett.* **35,** 1965–1967 (2010).
104. Birkholz, S. *et al.* Spatiotemporal rogue events in optical multiple filamentation. *Phys. Rev. Lett.* **111,** 243903 (2013).
105. Höhmann, R., Kuhl, U., Stöckmann, H. J., Kaplan, L. & Heller, E. J. Freak waves in the linear regime: A microwave study. *Phys. Rev. Lett.* **104,** 093901 (2010).
106. Arecchi, F. T., Bortolozzo, U., Montina, A. & Residori, S. Granularity and inhomogeneity are the joint generators of optical rogue waves. *Phys. Rev. Lett.* **106,** 153901 (2011).
107. The power of analogies. *Nature Photon.* **8,** 1 (2014).
108. Vergeles, S. & Turitsyn, S. K. Optical rogue waves in telecommunication data streams. *Phys. Rev. A* **83,** 061801 (2011).
109. Wabnitz, S. Optical tsunamis: Shoaling of shallow water rogue waves in nonlinear fibers with normal dispersion. *J. Opt.* **15,** 064002 (2013).
110. Bendahmane, A., Vanvincq, O., Mussot, A. & Kudlinski, A. Control of the soliton self-frequency shift dynamics using topographic optical fibers. *Opt. Lett.* **38,** 3390–3393 (2013).
111. Droques, M. *et al.* Fourth-order dispersion mediated modulation instability in dispersion oscillating fibers. *Opt. Lett.* **38,** 3464–3467 (2013).
112. Chabchoub, A., Hoffmann, N. P. & Akhmediev, N. Rogue wave observation in a water wave tank. *Phys. Rev. Lett.* **106,** 204502 (2011).
113. Chabchoub, A., Hoffmann, N., Onorato, M. & Akhmediev, N. Super rogue waves: Observation of a higher-order breather in water waves. *Phys. Rev. X* **2,** 011015 (2012).
114. Onorato, M., Proment, D., Clauss, G. & Klein, M. Rogue waves: From nonlinear Schrödinger breather solutions to sea-keeping test. *PLoS ONE* **8,** e54629 (2013).
115. Dysthe, K. B. Note on a modification to the non-linear Schrödinger-equation for application to deep-water waves. *P. Roy. Soc. Lond. A Mat.* **369,** 105–114 (1979).
116. Dias, F. & Kharif, C. Nonlinear gravity and capillary-gravity waves. *Ann. Rev. Fluid Mech.* **31,** 301–346 (1999).
117. Zakharov, V. E. & Dyachenko, A. I. About shape of giant breather. *Eur. J. Mech. B* **29,** 127–131 (2010).
118. Chabchoub, A. *et al.* Hydrodynamic supercontinuum. *Phys. Rev. Lett.* **111,** 054104 (2013).

Acknowledgements

J.M.D. and F.D. acknowledge the European Research Council Advanced Grant ERC-2011-AdG-290562 MULTIWAVE. J.M.D. also acknowledges support from the Agence Nationale de la Recherche project ANR-12-BS04-0011-05 OPTIROC. F.D. also acknowledges the Science Foundation Ireland grant SFI/12/ERC/E2227. M.E. acknowledges the Marsden Fund of the Royal Society of New Zealand. G.G. acknowledges the Academy of Finland Grants 130 099 and 132 279.

Author contributions

All authors contributed equally to the writing of this work.

Additional information

Reprints and permissions information is available online at www.nature.com/reprints. Correspondence and requests for materials should be addressed to G.G.

Competing financial interests

The authors declare no competing financial interests.